

P3P: Pseudo-3D Pre-training for Scaling 3D Masked Autoencoders

Xuechao Chen¹, Ying Chen², Jialin Li², Qiang Nie^{4,2}, Hanqiu Deng², Yong Liu², Qixing Huang³, Yang Li^{1*}

¹SIGS, Tsinghua University ²Youtu Lab, Tencent ³The University of Texas at Austin

⁴Hong Kong University of Science and Technology (Guangzhou)

Abstract

Pre-training in 3D is pivotal for advancing 3D perception tasks. However, the scarcity of clean 3D data poses significant challenges for scaling 3D pre-training efforts. Drawing inspiration from semi-supervised learning, which effectively combines limited labeled data with abundant unlabeled data, we introduce an innovative self-supervised pre-training framework. This framework leverages both authentic 3D data and pseudo-3D data generated from images using a robust depth estimation model. Another critical challenge is the efficiency of the pre-training process. Existing approaches, such as Point-BERT and Point-MAE, utilize k -nearest neighbors for 3D token embedding, resulting in quadratic time complexity. To address this, we propose a novel token embedding strategy with linear time complexity, coupled with a training-efficient 2D reconstruction target. Our method not only achieves state-of-the-art performance in 3D classification, detection, and few-shot learning but also ensures high efficiency in both pre-training and downstream fine-tuning processes.

1. Introduction

3D perception using 3D sensors such as LiDAR and depth cameras is a fundamental task for interpreting and interacting with the physical world in fields such as robotics and augmented reality. Current approaches for 3D perception usually require abundant real and clean 3D data to effectively pre-train a 3D model, which is then adapted for various downstream perception tasks, such as 3D detection, 3D classification, etc. To construct pre-training datasets, most 3D pre-training methods [40, 25, 42, 6, 37] employ complete 3D objects [2] or completely reconstructed 3D scenes from RGB-D scans. These approaches, however, are costly, as reconstructing targets from 3D RGB-D [2] scans inevitably introduces noise and artifacts, which require human effort for correction. This limitation results in a lack of size and diversity in the pre-training data. Moreover, the collection

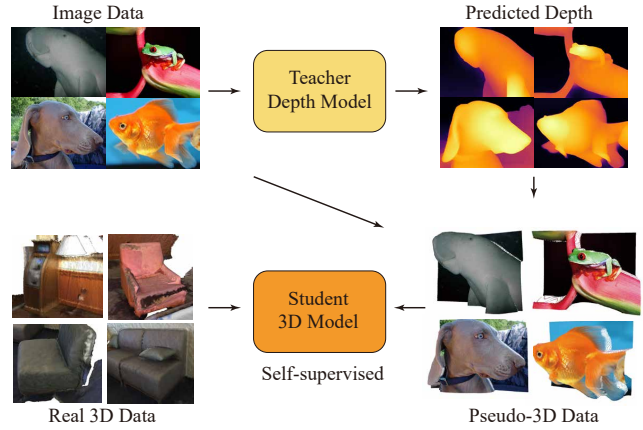


Figure 1: We propose Pseudo-3D Pre-training (P3P) to introduce the diversity of 2D images into 3D self-supervised pre-training. The 3D geometry knowledge is distilled from a teacher depth model.

of complete dynamic 3D objects and the reconstruction of dynamic 3D scenes from the real world present even greater challenges.

In this work, we approach the data-scale issue in 3D pre-training by offline distilling the 3D geometric knowledge from a depth estimation foundation model to a 3D model. A recent work, Depth Anything [38, 39], trained large depth estimation models that were semi-supervised on labeled depth images and unlabeled images. Their superior performance of estimating depth from a single image is conspicuous, as illustrated in Fig. 1. By combining the predicted depth and the original image, we obtain pseudo-3D data, namely pseudo RGB-D scans. In our work, we consider the large depth model as a teacher model producing pseudo-3D data for self-supervised pre-training. Since the RGB-D scans are the easiest real 3D data to acquire and the most similar data to the lifted pseudo-3D data, we take it into another source of our 3D self-supervised pre-training corpora. In the real world, the number of images is nearly unlimited, while the number of collected RGB-D scans is limited. Therefore, we organize the two sources of pre-training corpora as a mix of

*Corresponding author

millions of pseudo-3D data and tens of thousands of real 3D data.

Another challenge in pre-training using a large amount of pseudo-3D data is the pre-training efficiency. Masked Autoencoders (MAE) [15] is a popular 2D image pre-training method, as it has been proven effective in capturing the underlying data distribution and preserving the spatial information of the input data. Although MAE has been applied in 3D pre-training in works such as Point-MAE [25], it suffers from poor computation efficiency of 3D token embedding, which is accomplished through clustering using the k nearest neighbors (KNN), requiring quadratic time complexity. To illustrate the importance of reducing the token embedding time complexity for large-scale pseudo-3D pretraining, let's take ImageNet-1K [29], the 2D data source we ultimately used, as an example. Using an off-the-shelf depth estimation model, we lift over a million images from 2D space to 3D space, treating every pixel in each image as a 3D point. A typical image from ImageNet-1K usually contains $500 \times 350 = 175,000$ pixels. When applying point-based and KNN models like Point-BERT [40] and Point-MAE [25], it requires about $175,000 \times 175,000 = 30,625,000,000$ calculations, which is quite substantial for just a single image! In contrast, voxel-based methods [24, 14, 7] typically require near-linear time complexity to embed 3D tokens through discrete coordinate hashing. We designed a voxel-based 3D token embedding method, Sparse Weight Indexing, which has only a linear time complexity. To the best of our knowledge, ours is the first work to use an MAE paradigm with a linear complexity token embedding scheme in 3D model pre-training.

Finally, to further improve the efficiency of the MAE paradigm for pre-training 3D models, we designed a more efficient reconstruction target. We observed that both pseudo and real RGB-D scans can be regarded as 2D images with features x, y, z, r, g, b , where x, y, z represent 3D position information and r, g, b correspond to colors. This observation allows us to design a 2D reconstruction target, which considerably reduces the computational cost. As a result, we scaled up point cloud pre-training from thousands of points to 100,000 points, enabling the utilization of a larger amount of pre-training corpora and better scalability for downstream tasks involving large-scale point clouds. Extensive experiments demonstrate the efficacy and efficiency of our proposed methods. We also achieve state-of-the-art performance on 3D classification and few-shot classification among MAE-based pre-training methods.

In summary, the main contributions of our work are as follows:

- We propose a novel self-supervised pre-training method called P3P, which successfully leverages large-scale pseudo-3D data along with limited real 3D data to enhance the pre-training of 3D transformers.

- We introduce a highly efficient 3D token embedding strategy, Sparse Weight Indexing, to directly perform weight indexing based on voxel representation.
- We design an efficient 2D reconstruction target for 3D pre-training, which can reduce the calculation space from cubic to quadratic while maintaining downstream task performance.

2. Related Work

2.1. 3D Pre-training

Before the Masked Autoencoders (MAE) trends in 3D pre-training, PointContrast [36] proposed an unsupervised pre-text task for 3D pre-training. It learns to distinguish between positive and negative point pairs, where positive pairs come from the same object or scene, and negative pairs come from different objects or scenes. Later OcCo [34] proposed an unsupervised point cloud pre-training, feeding the encoder with a partial point cloud and making the decoder predict the whole point cloud.

Point-BERT introduces a masked 3D pre-training and provides a solid codebase upon which enables the followers to build their methods. Based on Point-BERT, Point-MAE extends the MAE pre-training method to the 3D point cloud. Point-M2AE [42] proposes multi-scale masking pre-training making the model learn hierarchical 3D features. Following the 3D patch embedding used by Point-BERT, Point-MAE, and Point-M2AE, PointGPT [6] proposes an auto-regressively generative pre-training method for point cloud learning. They both pre-train their transformers on the ShapeNet [4] dataset, containing around 50,000 unique 3D models from 55 common object categories, which has limitations in pre-training data size and the 3D token embedding strategy.

2.2. 2D & 3D Joint Pre-training

There are some recent work that focus on jointly pre-training on 2D and 3D data. Joint-MAE [12] leverages the complementary information in 2D images and 3D point clouds to learn more robust and discriminative representations. Multiview-MAE [8] is trained to reconstruct 3D point clouds from multiple 2D views and vice versa. This allows the model to capture the inherent correlations between 3D and 2D data. SimIPU [21] leverages the inherent spatial correlations between 2D images and 3D point clouds to learn spatial-aware visual representations. PiMAE [5] and Inter-MAE [23] are trained to reconstruct the original data from one modality (e.g., point cloud) using the information from the other modality (e.g., image). This allows the model to capture the inherent correlations between the two modalities. These methods focus on distillation from 2D pre-trained models or learning from the correspondence between 2D and 3D.

2.3. Learning From Pseudo Data

MixMatch [3] proposes the MixUp method to leverage limited real labeled data and a large amount of pseudo-labeled data. Their simple but effective mixing-up method enlightens us in this work. Depth Anything and Segment Anything [19] also enlarges their pre-training data scale in a semi-supervised and distillation manner. Their models rely on limited labeled data and a large amount of unlabeled data. They leverage unlabeled data by generating pseudo labels using a teacher model, which is an offline distillation from the teacher model to the student model, achieving excellent performance, which inspires us in this work. Moreover, recent findings [41, 6] in self-supervised pre-training also indicate that large models’ performance is strongly correlated with the scale of pre-training data. Therefore, in this work, we propose P3P leveraging the generated pseudo-3D data to pre-train our MAE models.

3. Approach

In this section, we briefly introduce the self-supervised pre-training method of Masked Autoencoders at the beginning. Then we detail the difference in our approach, including image lifting, embedding, and reconstruction target.

Preliminaries. Masked Autoencoders (MAE) method formulates the image self-supervised pre-training as a token masking and reconstruction problem. At first, an image of the resolution 224×224 is partitioned into $14 \times 14 = 196$ patches with a patch size of 16×16 . Each image patch of the resolution 16×16 is embedded by multiplying with 16×16 corresponding learnable weights. Second, the embedded 196 tokens of an image are randomly masked, and only a small part of visible tokens are fed into a transformer encoder. Third, the encoded visible tokens are fed to a transformer decoder with the masked empty tokens together. The decoder is targeted at reconstructing all pixels in the masked tokens. Mean squared error (MSE) is used to supervise the pre-training process, recovering the masked RGB pixels. Later, Point-MAE extends the MAE pre-training from images to point clouds. The main difference between Point-MAE and MAE lies in the token embedding and the reconstruction target. Point-MAE changes the original MSE supervision to Chamfer Distance [11].

3.1. Data Creation

To leverage any 2D images to pre-train 3D models, we choose the ImageNet-1K (IN1K) [29] without any depth annotations as our basic dataset. One advantage of lifting 2D images to 3D is the much larger data size and better diversity compared with point clouds collected by depth cameras, LiDAR, or sampled from 3D CAD models. Another advantage is the labor-saving for the reconstruction

of 3D complete objects or scenes. The third advantage lies in the small domain gap with real RGB-D scans. Inspired by MixMatch, mixing up pseudo-labeled data and manually labeled data with a mixing ratio to perform semi-supervised training. We directly mix up the two data sources for our self-supervised learning. We surprisingly find that the direct mixing is simple yet effective, as demonstrated in our experiment section.

We employ an off-the-shelf large model Depth Anything [38], which is trained on labeled depth images and unlabeled images. We denote it as f for depth estimation, lifting 2D images into 3D canonical space. The self-supervised learning performed on the lifted pseudo-3D data can be regarded as offline distillation, introducing abundant 3D geometry information to our model, as shown in Fig. 1. Given an image I , we obtain a lifted pseudo-3D point cloud $P = \phi(I, f(I)) = \{p_i = [x_i, y_i, z_i, r_i, g_i, b_i] | i = 1, 2, 3, \dots, N\}$, where x_i, y_i, z_i are the normalized continuous coordinates and r_i, g_i, b_i are the normalized colors of each point p_i corresponding to each pixel in image I . ϕ maps the 2D coordinates of the image I to 3D according to depth $f(I)$. For a 3D coordinate system in robotics, one of the conventions is to portray the xy-plane horizontally, with the z-axis added to represent the height (positive up). In this paper, we keep this convention. Since most of the images in ImageNet are taken from the horizontal views, we assign the predicted depth of the image to the y-axis. The height of the image is aligned with the z-axis and the width of the image is aligned with the x-axis.

3.2. Embedding

To scale up our model for large point clouds (over 100K points per point cloud), learning the context information for the detection task, we do not employ the popular token embedding strategy used by Point-BERT [40], Point-MAE [25], Point-M2AE [42], and PointGPT [6], which use low-efficient Farthest Point Sampling and k nearest neighbor to build 3D patches, and employ a pre-trained PointNet [27] to embed 3D tokens. These strategies are not scalable to large point clouds. Instead, we follow the token embedding implemented in the vision transformers [10] and extend it to 3D based on the voxel representation. Given a point cloud P , the voxelization ψ processes the continuous coordinates x, y, z and produces the discrete coordinates m, n, q for voxels:

$$(m, n, q) = (\lfloor x/s \rfloor, \lfloor y/s \rfloor, \lfloor z/s \rfloor), \quad (1)$$

where $\lfloor \cdot \rfloor$ denotes floor function and s is the basic voxel size much less than the maximum value of x, y, z . Since one voxel may contain many points, we simply choose the point with the maximum value of features to represent the voxel. The voxel set V representing the whole point cloud can be written as: $V = \psi(P) = \{v_{m_i, n_i, q_i} =$

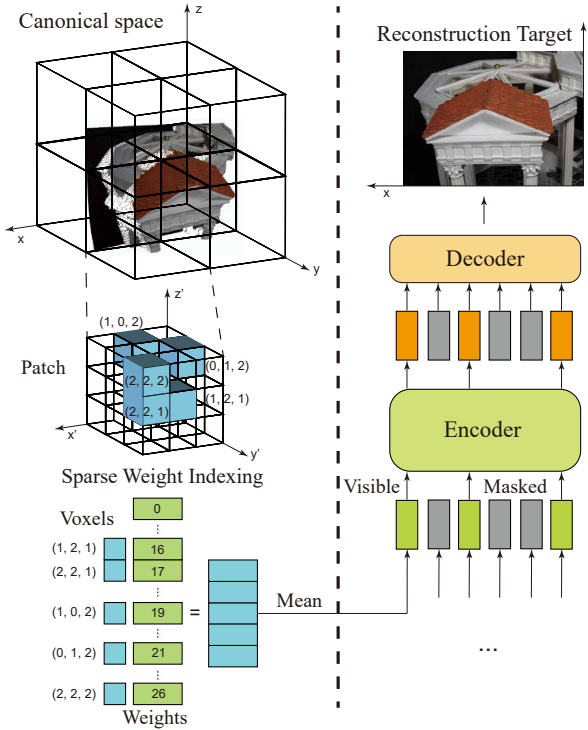


Figure 2: Overall pipeline of our pre-training approach. The left part shows how our proposed Sparse Weight Indexing embeds 3D tokens. The right part shows the MAE pre-training paradigm with an innovative 2D reconstruction target for 3D pre-training.

$[x_i, y_i, z_i, r_i, g_i, b_i] | i = 1, 2, 3, \dots, M, M \leq N\}$. Given range limits, the discretized 3D space is divided into multiple 3D patches as illustrated in Fig. 2, we use the 3D patch $V_{a,a,0} \subset V$ that satisfies $\forall v_{m_i, n_i, q_i} \in V_{a,a,0}, a \leq m_i, n_i < 2a, 0 \leq q_i < a$, where a is the basic size of each 3D patch, as an example. In our model, we fix a to 16. Recall that, in 2D vision transformers, each token owns a corresponding positional embedding representing its global position. For 3D point clouds, we can directly use the minimum corner's 3D coordinates to represent the position of each 3D patch. Thus, the position of patch $V_{a,a,0}$ is $(a, a, 0)$. We employ linear layers with GELU [16] for positional embedding, which maps the coordinates to high-dimensional feature space. Following MAE [15], the positional embedding for the encoder and decoder is learned independently.

To make the model grasp more geometry knowledge through MAE pre-training, we add some additional 3D information to the input feature set. We calculate the relative coordinates for each voxel v_{m_i, n_i, q_i} in patch $V_{a,a,0}$ and average the relative coordinates to get the 3D center of patch $V_{a,a,0}$:

$$(x'_i, y'_i, z'_i) = (x_i - a, y_i - a, z_i - 0), \quad (2)$$

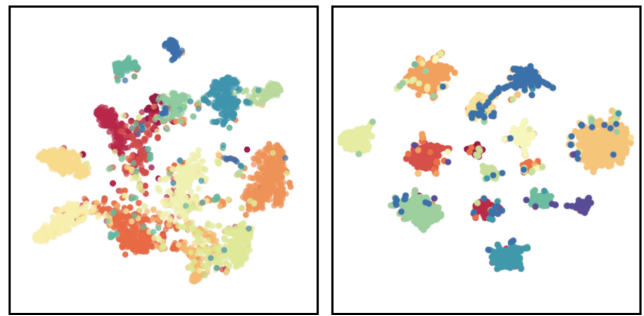


Figure 3: Visualization of feature distributions. We show the t-SNE visualization of feature vectors after fine-tuning on the ScanObjectNN PB_T50_RS classification dataset. We make a comparison between Point-BERT(left) and ours(right).

$$(\bar{x}', \bar{y}', \bar{z}') = \left(\frac{1}{L} \sum_{i=1}^L x'_i, \frac{1}{L} \sum_{i=1}^L y'_i, \frac{1}{L} \sum_{i=1}^L z'_i \right). \quad (3)$$

where L is the number of all voxels in patch $V_{a,a,0}$. Finally, the enhanced 3D patch $V'_{a,a,0}$ is denoted as: $V'_{a,a,0} = \{v'_{m_i, n_i, q_i} = [x_i, y_i, z_i, r_i, g_i, b_i, x'_i, y'_i, z'_i, \bar{x}', \bar{y}', \bar{z}'] | i = 1, 2, 3, \dots, L, L < M\}$.

The 3D patch $V'_{a,a,0}$ is now ready for token embedding. We employ a^3 trainable weights to embed $V'_{a,a,0}$, which follows 2D token embedding implemented by vision transformers [10] and MAE [15] but different in data input. For 2D image patches, the data is dense and thus can use dense calculation, i.e., 2D convolution with a large kernel and stride. In contrast, 3D point clouds and their discrete voxels are sparse data that is better to be calculated sparsely. Therefore, we propose Sparse Weight Indexing (SWI) to index the a^3 weights in L sparse voxels. For $v'_{m_i, n_i, q_i} \in V'_{a,a,0}$, we calculate the index d_i of the weights as

$$d_i = (m_i \% a) + (n_i \% a) + (q_i \% a)a^2, \quad (4)$$

where $a \leq m_i, n_i < 2a, 0 \leq q_i < a$, and $(\% a)$ calculates the remainder of $*$ divided by a . It is easy to see that $0 \leq d_i < a^3$. Thus, we only need a^3 shared trainable weights to extract the 3D features of all 3D patches. Each weight $w_{d_i} \in \mathbb{R}^{12 \times C}$, where C is the embedding dimension. After 3D feature extraction, all the voxel features extracted in a 3D patch are averaged to the 3D token $T_{a,a,0}$,

$$T_{a,a,0} = \frac{1}{L} \sum_{i=1}^L v'_{m_i, n_i, q_i} w_{d_i}. \quad (5)$$

3.3. Masked Autoencoders Pre-training

As demonstrated in Fig. 2, the input 3D patches are first randomly masked. Second, the visible 3D patches are embedded into 3D tokens through the Sparse Weight Indexing

method. Third, the visible tokens are fed into a transformer encoder. Finally, the encoded visible tokens and the masked empty tokens are fed into a transformer decoder to reconstruct every voxel within each masked patch.

3.4. Reconstruction Target

Recall that our pre-training data contains the pseudo-3D scans lifted from 2D images along with the real RGB-D scans. Hence, each 3D voxel of the point cloud has a unique correspondence with each pixel on the camera plane. The 3D prediction needs to reconstruct a^3 voxels of the 3D masked token, which is very consuming in GPU memory. We simplify this prediction task as the 2D prediction of a^2 voxels by modeling the projection correspondence, reducing the calculation space from cubic to quadratic. We show in our experiment section that the 2D reconstruction target is sufficient for the self-supervised task on lifted 3D data.

As shown in Fig. 2, the height of the lifted image is aligned with the z-axis, and the width of the image is aligned with the x-axis. Thus we can project the 3D reconstruction target to the XZ-plane, regarding the voxels with 12 features as super pixels. Given a reconstruction target patch $V' = \{v'_i = [x_i, y_i, z_i, r_i, g_i, b_i, x'_i, y'_i, z'_i, \bar{x}', \bar{y}', \bar{z}'] | i = 1, 2, 3, \dots, a^2\}$, we project the 3D patch onto the XZ-plane and get a super-image patch.

$$I' = \begin{bmatrix} v'_{0,0} & v'_{0,1} & \dots & v'_{0,a-1} \\ v'_{1,0} & v'_{1,1} & \dots & v'_{1,a-1} \\ \dots & \dots & \dots & \dots \\ v'_{a-1,0} & v'_{a-1,1} & \dots & v'_{a-1,a-1} \end{bmatrix}. \quad (6)$$

The transformer decoder predicts the 2D patch \hat{I}' . Following MAE [15], after the prediction of a 2D image patch, we use the L2 loss to supervise relative features: $r_i, g_i, b_i, x'_i, y'_i, z'_i, \bar{x}', \bar{y}', \bar{z}'$. For the absolute features x_i, y_i, z_i , we follow Point-MAE [25] and employ Chamfer Distance [11] as supervision. We show in our experiment section that the hybrid loss is more effective than using L2 loss only.

4. Experiment

4.1. Pre-training

Model. The pre-training transformer encoder is the same as the model used in the pre-training methods listed in Tab 1 except Point-M2AE. Point-M2AE has 15 transformer blocks, while ours and other pre-training methods listed in Tab 1 only have 12 transformer blocks. The pre-training transformer decoder is the same as the decoder used in MAE, containing 8 transformer blocks.

Pre-training data and settings. Similar to semi-supervised settings incorporating real and pseudo labels, the

overall pre-training data consists of pseudo-3D scans lifted from images and real RGB-D scans sampled from the ScanNet [9] training set. For the first part of the pre-training data, we lift the images from ImageNet-1K (IN1K) [29] training set using the off-the-shelf large depth estimation model V1 large [38] and its second version V2 large [39]. Most of the images have a resolution of 500×350 , leading to 175,000 points after the lifting. The total number of pseudo-3D data is 1.28 million. For the second part of the pre-training data, we sample from the ScanNet training set at a sampling stride of 100, which leads to a total number of 25,000 scans. We randomly mix up the two parts of data to pre-train our final model. Data augmentation, including horizontal flip and rotation, is employed during pre-training.

We load the pre-trained parameters of the MAE encoder before our pre-training to have a good parameter initialization. The masking ratio in MAE is set to 60%. We provide 3 versions of the pre-trained transformer encoder: 1) pre-training based on Depth Anything V1 pseudo-3D data and ScanNet real 3D data, with a down-sampling point number $2K$; 2) pre-training based on Depth Anything V1 pseudo-3D data and ScanNet real 3D data, with a down-sampling point number $100K$; 3) pre-training based on Depth Anything V2 pseudo-3D data and ScanNet real 3D data, with a down-sampling point number $2K$. We pre-train our models on 8 V100 (32GB) GPUs for 100 epochs. We use AdamW as the optimizer with a start learning rate of $5e-4$ and a cosine learning rate scheduler. For the $2K$ version model, the total batch size is set to 128, and we update the parameters every 8 iters. For the $100K$ version model, the total batch size is set to 64, and we update the parameters every 16 iters.

4.2. Downstream Tasks

3D classification. 3D classification takes the 3D point cloud of an object as input and predicts a class label for the object. The pre-trained transformer encoder is followed by a classification head (one linear layer), and the decoder is discarded in the same setting as previous MAE-based methods. At the fine-tuning stage, we fine-tune all the parameters in the pre-trained transformer encoder. We take the class token as the input for the classification head. The supervision loss is the Cross Entropy Loss.

We choose ScanObjectNN [33] as the dataset of our downstream classification tasks. ScanObjectNN contains 2902 scanned objects from the real world that are categorized into 15 classes. The raw objects own a list of points with coordinates, normals, and colors. In our setting, we only use the coordinates and colors, counting 6 original features. ScanObjectNN has multiple splits of data. We choose to use the main split following previous methods. For the base version of the data, 2902 objects can be fed with background or not, denoted as OBJ_BG or OBJ_ONLY. The hardest version of the data is denoted as PB_T50_RS, which augments

Method	Pre-train	Points	ScanObjectNN		
			OBJ_BG	OBJ_ONLY	PB_T50_RS
PointNet [27]	✗	2K	73.3	79.2	68.0
DGCNN [35]	✗	2K	82.8	86.2	78.1
PointCNN [20]	✗	2K	86.1	85.5	78.5
MVTN [13]	✗	2K	92.6	92.3	82.8
Point-BERT [40]	✓	1K	87.4	88.1	83.1
MaskPoint [22]	✓	2K	89.3	88.1	84.3
Point-MAE [25]	✓	2K	90.0	88.2	85.2
Point-M2AE [42]	✓	2K	91.2	88.8	86.4
PointGPT [6]	✓	2K	91.6	90.0	86.9
MVNet [37]	✓	-	91.4	89.7	86.7
P3P (V1 Large)	✓	2K	93.1	91.4	86.4
P3P (V2 Large)	✓	2K	93.8	91.7	87.9

Table 1: Classification results on ScanObjectNN dataset. The highest accuracy is shown in bold for supervised methods and pre-trained methods separately. “Points” represents the number of points taken as input.

Pre-training Method	5-way		10-way	
	10-shot	20-shot	10-shot	20-shot
Rand	62.0±5.6	67.8±5.1	37.8±4.3	41.8±2.4
Jigsaw [30]	65.2±3.8	72.2±2.7	45.6±3.1	48.2±2.8
cTree [31]	68.4±3.4	71.6±2.9	42.4±2.7	43.0±3.0
OcCo [34]	72.4±1.4	77.2±1.4	57.0±1.3	61.6±1.2
CrossPoint [1]	74.8±1.5	79.0±1.2	62.9±1.7	73.9±2.2
Point-BERT [40]	78.7±4.1	83.1±5.8	65.0±5.1	74.4±4.0
P3P	81.4±5.3	84.2±5.4	69.8±4.3	75.1±4.3

Table 2: Few-shot object classification results on ScanObjectNN. We report mean and standard error over 10 runs. This table is an extended version from [1].

each object 5 times by translation, rotation, and scaling. In this version, there are 14,510 perturbed objects with backgrounds in total.

We fine-tune the two pre-trained versions (2K V1 large, 2K V2 large) on OBJ_BG, OBJ_ONLY, and PB_T50_RS separately, comparing with previous methods in Tab. 1. We surpass the previous methods distinctly and achieve state-of-the-art accuracy among mask-based pre-training methods. We show the t-SNE visualization after fine-tuning in Fig. 3, comparing it with Point-BERT. Ours (right) is more distinct between the 15 categories and more cohesive within each category, showing the advantage of our pre-training.

Few-shot classification. Few-shot learning aims to train a model that generalizes with limited data. We evaluate our model on ScanObjectNN OBJ_BG. We strictly follow CrossPoint [1] and conduct experiments on conventional few-shot tasks (N-way K-shot), where the model is evaluated on N classes, and each class contains K samples. As shown

in Tab. 2, we outperform CrossPoint by a large margin and achieve new state-of-the-art performance, showing the strong generalization ability of our model. For fair comparison, we test the pre-trained Point-BERT model.

3D detection. 3d detection task predicts 3D bounding boxes and categories for every object in the 3D scene. The pre-trained transformer encoder is followed by VoteNet [26], and the transformer decoder is discarded, as in the same setting as MAE.

ScanNet contains 2.5M camera sequences in 1513 scenes with 36,213 annotated objects. The dataset contains RGB-D video sequences, which are color (RGB) videos with an additional depth camera that provides information about the distance of objects from the camera. SUN RGB-D [32] is another indoor dataset containing 64,595 3D bounding boxes with accurate object orientations. The dataset is collected from a variety of indoor scenes, including homes, offices, classrooms, stores, and more.

Pre-training Method	ScanNet		SUN RGB-D	
	mAP@0.25	mAP@0.5	mAP@0.25	mAP@0.5
STRL [18]	59.5	38.4	58.2	35.0
Point-BERT [40]	61.0	38.3	-	-
RandomRooms [28]	61.3	36.2	59.2	35.4
MaskPoint [22]	63.4	40.6	-	-
PointContrast [36]	59.2	38.0	57.5	34.8
DepthContrast [43]	62.1	39.1	60.4	35.4
SceneContext [17]	-	39.3	-	36.4
MVNet[37]	64.0	41.5	62.0	39.6
P3P (2K version)	64.5	44.7	60.2	36.3
P3P (100K version)	65.4	45.2	61.0	37.1

Table 3: Comparison of 3D object detection results with pre-training methods. We show mean Average Precision (mAP) across all semantic classes with 3D IoU thresholds of 0.25 and 0.5. The highest and second highest results are shown in bold.

As shown in Tab. 3, we choose VoteNet as our detection framework following the listed previous pre-training methods. We outperform all the listed previous pre-training methods on the ScanNet dataset. The input point number is $40K$ because ScanNet is a large-scale dataset. On the SUN RGB-D dataset, the recent work MVNet is higher than ours, while ours achieves the second highest, and we surpass a bundle of other previous methods. The input point number is $100K$. We find that the pre-trained $2K$ version is less effective than the $100K$ version because the detection scene is large-scale and requires context information. The pre-trained model grasps better context knowledge when pre-training with $100K$ points than when pre-training with $2K$ points.

4.3. Ablation Study

In this section, we conduct experiments to find the best settings for our approach. We explore the impact of input features, loss design, reconstruction target, pre-training based on the two token embedding strategies, token embedding efficiency, masking ratio, data scaling, and mixing ratio. For different control experiments, we independently pre-train our model with a sampling of $2K$ points. We evaluate our model on the classification task of ScanObjectNN OBJ_BG. At the fine-tuning stage, we fine-tune all the parameters in the pre-trained transformer encoder.

Input features. The original features of the input point cloud include coordinates x, y, z , and colors r, g, b . We run an experiment pre-training only on the original 6 features. As shown in Tab. 4a, the 12 enhanced features surpass the 6 original features by 1.62% accuracy.

Loss design. We conduct an ablation study on the L2 loss designed in MAE. As shown in Tab. 4a, our hybrid loss achieves 2.44% higher accuracy than L2 loss only.

Reconstruction target. We compare the reconstruction target to recover 3D space with to recover 2D space. As shown in Tab. 4b, the 3D reconstruction target is slightly worse than the 2D reconstruction target, which shows the 2D reconstruction target is sufficient in our pre-training. Meanwhile, we save the pre-training time and GPU memory by a large margin.

Pre-training based on the two token embedding strategies. We make thorough comparisons between our token embedding and the token embedding implemented in Point-BERT and Point-MAE. We denote F-K-P as their token embedding, namely “farthest point sampling”-“ k nearest neighbors”-“PointNet”. Ours is denoted as V-P-S, namely “voxelization”-“partition patches”-“Sparse Weight Indexing”. Note that we keep the original F-K-P implementation, which is running on GPU devices with an accelerating CUDA library. Ours is also implemented on GPU devices. Therefore, the efficiency comparison is fair and meaningful. As shown in Tab. 4b, the evaluation results are close, but the pre-training time and GPU memory are saved distinctly, showing the efficiency of our proposed V-P-S token embedding strategy.

Token embedding efficiency To further demonstrate the efficiency of our V-P-S token embedding, we make comparisons of embedding different numbers of points and tokens with F-K-P, as shown in Tab. 4c. For both of the embedding strategies, we keep the embedding dimension.

Note that the calculation index “FLOPs” (floating point of operations) can reflect the time complexity regardless of CPU/GPU devices. When fed with 2,048 points, F-K-P needs $2,829M$ FLOPs while ours only needs $75M$ FLOPs, reducing the calculation by 37 times. When fed with 32,768 points, F-K-P needs $45,315M$ FLOPs while ours only needs

origin	enhance	L2	Chamfer	ACC(%)	3D	2D	F-K-P	V-P-S	epoch time	GPU mem.	ACC(%)
✓		✓	✓	86.71	✓			✓	2321 s	123 GB	88.09
✓	✓	✓	✓	88.33		✓		✓	1742 s	75 GB	88.33
✓	✓			85.89		✓	✓		2693 s	131 GB	88.16
(a)						(b)					
Strategy	points	tokens	FLOPs	reduction ratio			Ratio (%)	ACC(%)			
F-K-P	2,048	64	2,829M	-			15	86.79			
	12,544	196	17,342M	-			30	87.13			
	32,768	256	45,315M	-			45	88.16			
V-P-S(ours)	2,048	64	75M	$\times 37$			60	88.33			
	12,544	196	232M	$\times 74$			75	86.62			
	32,768	256	303M	$\times 149$			90	83.70			
(c)						(d)					
Data type	12K	25K	500K	1M	Real:Pseudo	12K:1M	25K:1M	25K:500K	25K:50K		
Real	42.19	75.12	-	-							
Pseudo	36.19	40.13	84.56	88.33	ACC(%)	88.57	89.19	85.62	77.23		
(e)						(f)					

Table 4: Ablation study of our design choices. The evaluation metric is the accuracy on the ScanObjectNN OBJ_BG. (a) Input features and loss design (b) Pre-training based on the two reconstruction targets and two token embedding strategies (c) Token embedding efficiency (d) Masking ratio (e) Data scaling (f) Mixing ratio.

303M FLOPs, reducing the calculation by 149 times. The results show our strong computing efficiency.

Masking ratio. Random masking is an effective masking strategy according to MAE and Point-MAE. We pre-train our model with different masking ratios to find the best setting. As shown in Tab. 4d, we find the masking ratio of 60% achieves the highest accuracy on the downstream classification task. When the masking ratio increases, the accuracy drops faster than when it decreases.

Data scaling. We show in Tab. 4e that 1) both real and pseudo-3D pre-training corpora accord with data scaling law; 2) real 3d data performs more effectively than pseudo-3D data at the same data scale; 3) pseudo-3D data leads to the significant performance increase when the data size comes to over 500K. It is worth noting that in the real world, images are much easier to acquire than real 3D RGB-D scans, leading to pseudo-3D data being much more diverse than real 3D RGB-D scans. Although real 3D data gives more valuable geometry information, there is always a huge data gap between the amount of real 3D data and images/pseudo-3d. We believe large depth models can be a bridge to cross this huge data quantity gap.

Mixing ratio. We mix up the real RGB-D scans and the pseudo-3D scans to find whether the real data and the pseudo data can benefit the 3D pre-training together in a mix-up way. When we use all the 25K real scans and all the 1M pseudo scans, the accuracy reaches the highest of 89.19%. Whether we decrease the real or pseudo scans, the accuracy drops. This experiment shows the importance of both the real scans and the pseudo scans.

5. Conclusion

In this paper, we have reviewed recent progress in 3D pre-training, discussing key issues from a data-driven perspective. We have proposed an approach based on MAE leveraging pseudo-3D data lifted from images, introducing the large diversity into 3D space. To efficiently utilize the large-scale data, we have proposed a novel 3D token embedding strategy and a 2D reconstruction target. Both of the proposed accelerate the pre-training greatly. We have conducted downstream experiments demonstrating the effectiveness of our pre-training approach, reaching state-of-the-art performance on classification and few-shot learning. The detection experiment shows the importance of scaling up the point number feeding to a transformer. We also do different ablation studies to reveal the nature and enlighten future research.

References

- [1] Mohamed Afham, Isuru Dissanayake, Dinithi Dissanayake, Amaya Dharmasiri, Kanchana Thilakarathna, and Ranga Rodriguez. Crosspoint: Self-supervised cross-modal contrastive learning for 3d point cloud understanding. In *Proceedings of the IEEE/CVF Conference on Computer Vision and Pattern Recognition*, 2022.
- [2] Iro Armeni, Sasha Sax, Amir R Zamir, and Silvio Savarese. Joint 2d-3d-semantic data for indoor scene understanding. *arXiv preprint arXiv:1702.01105*, 2017.
- [3] David Berthelot, Nicholas Carlini, Ian Goodfellow, Nicolas Papernot, Avital Oliver, and Colin A Raffel. Mixmatch: A holistic approach to semi-supervised learning. *Advances in neural information processing systems*, 2019.
- [4] Angel X Chang, Thomas Funkhouser, Leonidas Guibas, Pat Hanrahan, Qixing Huang, Zimo Li, Silvio Savarese, Manolis Savva, Shuran Song, Hao Su, et al. Shapenet: An information-rich 3d model repository. *arXiv preprint arXiv:1512.03012*, 2015.
- [5] Anthony Chen, Kevin Zhang, Renrui Zhang, Zihan Wang, Yuheng Lu, Yandong Guo, and Shanghang Zhang. Pimae: Point cloud and image interactive masked autoencoders for 3d object detection. In *Proceedings of the IEEE/CVF Conference on Computer Vision and Pattern Recognition*, 2023.
- [6] Guangyan Chen, Meiling Wang, Yi Yang, Kai Yu, Li Yuan, and Yufeng Yue. Pointgpt: Auto-regressively generative pre-training from point clouds. In *Advances in Neural Information Processing Systems*, 2023.
- [7] Xuechao Chen, Shuangjie Xu, Xiaoyi Zou, Tongyi Cao, Ditian Yan Yeung, and Lu Fang. Svqnet: Sparse voxel-adjacent query network for 4d spatio-temporal lidar semantic segmentation. In *Proceedings of the IEEE/CVF International Conference on Computer Vision*, 2023.
- [8] Zhimin Chen, Yingwei Li, Longlong Jing, Liang Yang, and Bing Li. Point Cloud Self-supervised Learning via 3D to Multi-view Masked Autoencoder. *arXiv preprint arXiv:2311.10887*, 2023.
- [9] Angela Dai, Angel X Chang, Manolis Savva, Maciej Halber, Thomas Funkhouser, and Matthias Nießner. Scannet: Richly-annotated 3d reconstructions of indoor scenes. In *Proceedings of the IEEE conference on computer vision and pattern recognition*, 2017.
- [10] Alexey Dosovitskiy, Lucas Beyer, Alexander Kolesnikov, Dirk Weissenborn, Xiaohua Zhai, Thomas Unterthiner, Mostafa Dehghani, Matthias Minderer, Georg Heigold, Sylvain Gelly, et al. An image is worth 16x16 words: Transformers for image recognition at scale. *arXiv preprint arXiv:2010.11929*, 2020.
- [11] Haoqiang Fan, Hao Su, and Leonidas J Guibas. A point set generation network for 3d object reconstruction from a single image. In *Proceedings of the IEEE conference on computer vision and pattern recognition*, 2017.
- [12] Ziyu Guo, Renrui Zhang, Longtian Qiu, Xianzhi Li, and Pheng-Ann Heng. Joint-mae: 2d-3d joint masked autoencoders for 3d point cloud pre-training. *arXiv preprint arXiv:2302.14007*, 2023.
- [13] Abdullah Hamdi, Silvio Giancola, and Bernard Ghanem. Mvtn: Multi-view transformation network for 3d shape recognition. In *Proceedings of the IEEE/CVF International Conference on Computer Vision*, 2021.
- [14] Chenhang He, Ruihuang Li, Shuai Li, and Lei Zhang. Voxel set transformer: A set-to-set approach to 3d object detection from point clouds. In *Proceedings of the IEEE/CVF conference on computer vision and pattern recognition*, 2022.
- [15] Kaiming He, Xinlei Chen, Saining Xie, Yanghao Li, Piotr Dollár, and Ross Girshick. Masked autoencoders are scalable vision learners. In *Proceedings of the IEEE/CVF conference on computer vision and pattern recognition*, 2022.
- [16] Dan Hendrycks and Kevin Gimpel. Gaussian error linear units (gelus). *arXiv preprint arXiv:1606.08415*, 2016.
- [17] Ji Hou, Benjamin Graham, Matthias Nießner, and Saining Xie. Exploring data-efficient 3d scene understanding with contrastive scene contexts. In *Proceedings of the IEEE/CVF Conference on Computer Vision and Pattern Recognition*, 2021.
- [18] Siyuan Huang, Yichen Xie, Song-Chun Zhu, and Yixin Zhu. Spatio-temporal self-supervised representation learning for 3d point clouds. In *Proceedings of the IEEE/CVF International Conference on Computer Vision*, 2021.
- [19] Alexander Kirillov, Eric Mintun, Nikhila Ravi, Hanzi Mao, Chloe Rolland, Laura Gustafson, Tete Xiao, Spencer Whitehead, Alexander C Berg, Wan-Yen Lo, et al. Segment anything. In *Proceedings of the IEEE/CVF International Conference on Computer Vision*, 2023.
- [20] Yangyan Li, Rui Bu, Mingchao Sun, Wei Wu, Xinhan Di, and Baoquan Chen. Pointcnn: Convolution on x-transformed points. In *Advances in neural information processing systems*, 2018.
- [21] Zhenyu Li, Zehui Chen, Ang Li, Liangji Fang, Qinhong Jiang, Xianming Liu, Junjun Jiang, Bolei Zhou, and Hang Zhao. Simipu: Simple 2d image and 3d point cloud unsupervised pre-training for spatial-aware visual representations. In *Proceedings of the AAAI Conference on Artificial Intelligence*, 2022.
- [22] Haotian Liu, Mu Cai, and Yong Jae Lee. Masked discrimination for self-supervised learning on point clouds. In *European conference on computer vision*, 2022.
- [23] Jiaming Liu, Yue Wu, Maoguo Gong, Zhixiao Liu, Qiguang Miao, and Wenping Ma. Inter-modal masked autoencoder for self-supervised learning on point clouds. *IEEE Transactions on Multimedia*, 2023.
- [24] Jiageng Mao, Yujing Xue, Minzhe Niu, Haoyue Bai, Jiashi Feng, Xiaodan Liang, Hang Xu, and Chunjing Xu. Voxel transformer for 3d object detection. In *Proceedings of the IEEE/CVF international conference on computer vision*, 2021.
- [25] Yatian Pang, Wenxiao Wang, Francis EH Tay, Wei Liu, Yonghong Tian, and Li Yuan. Masked autoencoders for point cloud self-supervised learning. In *European conference on computer vision*, 2022.
- [26] Charles R Qi, Or Litany, Kaiming He, and Leonidas J Guibas. Deep hough voting for 3d object detection in point clouds. In *proceedings of the IEEE/CVF International Conference on Computer Vision*, 2019.

[27] Charles R Qi, Hao Su, Kaichun Mo, and Leonidas J Guibas. Pointnet: Deep learning on point sets for 3d classification and segmentation. In *Proceedings of the IEEE conference on computer vision and pattern recognition*, 2017.

[28] Yongming Rao, Benlin Liu, Yi Wei, Jiwen Lu, Cho-Jui Hsieh, and Jie Zhou. RandomRooms: unsupervised pre-training from synthetic shapes and randomized layouts for 3D object detection. In *Proceedings of the IEEE/CVF International Conference on Computer Vision*, 2021.

[29] Olga Russakovsky, Jia Deng, Hao Su, Jonathan Krause, Sanjeev Satheesh, Sean Ma, Zhiheng Huang, Andrej Karpathy, Aditya Khosla, Michael Bernstein, Alexander C. Berg, and Li Fei-Fei. ImageNet Large Scale Visual Recognition Challenge. *International Journal of Computer Vision*, 2015.

[30] Jonathan Sauder and Bjarne Sievers. Self-Supervised Deep Learning on Point Clouds by Reconstructing Space. *Advances in Neural Information Processing Systems*, 2019.

[31] Charu Sharma and Manohar Kaul. Self-Supervised Few-Shot Learning on Point Clouds. In *Advances in Neural Information Processing Systems*, 2020.

[32] Shuran Song, Samuel P Lichtenberg, and Jianxiong Xiao. Sun rgb-d: A rgb-d scene understanding benchmark suite. In *Proceedings of the IEEE conference on computer vision and pattern recognition*, 2015.

[33] Mikaela Angelina Uy, Quang-Hieu Pham, Binh-Son Hua, Thanh Nguyen, and Sai-Kit Yeung. Revisiting point cloud classification: A new benchmark dataset and classification model on real-world data. In *Proceedings of the IEEE/CVF international conference on computer vision*, 2019.

[34] Hanchen Wang, Qi Liu, Xiangyu Yue, Joan Lasenby, and Matthew J. Kusner. Unsupervised Point Cloud Pre-Training via Occlusion Completion. In *International Conference on Computer Vision*, 2021.

[35] Yue Wang, Yongbin Sun, Ziwei Liu, Sanjay E Sarma, Michael M Bronstein, and Justin M Solomon. Dynamic graph cnn for learning on point clouds. *Acm Transactions On Graphics*, 2019.

[36] Saining Xie, Jiatao Gu, Demi Guo, Charles R Qi, Leonidas Guibas, and Or Litany. Pointcontrast: Unsupervised pre-training for 3d point cloud understanding. In *European Conference on Computer Vision*, 2020.

[37] Siming Yan, Chen Song, Youkang Kong, and Qixing Huang. Multi-View Representation is What You Need for Point-Cloud Pre-Training. In *The Twelfth International Conference on Learning Representations*, 2024.

[38] Lihe Yang, Bingyi Kang, Zilong Huang, Xiaogang Xu, Jiashi Feng, and Hengshuang Zhao. Depth Anything: Unleashing the Power of Large-Scale Unlabeled Data. In *Proceedings of the IEEE/CVF Conference on Computer Vision and Pattern Recognition*, 2024.

[39] Lihe Yang, Bingyi Kang, Zilong Huang, Zhen Zhao, Xiaogang Xu, Jiashi Feng, and Hengshuang Zhao. Depth Anything V2. *arXiv:2406.09414*, 2024.

[40] Xumin Yu, Lulu Tang, Yongming Rao, Tiejun Huang, Jie Zhou, and Jiwen Lu. Point-BERT: Pre-Training 3D Point Cloud Transformers With Masked Point Modeling. In *Proceedings of the IEEE/CVF International Conference on Computer Vision*, 2022.

[41] Xiaohua Zhai, Alexander Kolesnikov, Neil Houlsby, and Lucas Beyer. Scaling vision transformers. In *Proceedings of the IEEE/CVF conference on computer vision and pattern recognition*, 2022.

[42] Renrui Zhang, Ziyu Guo, Peng Gao, Rongyao Fang, Bin Zhao, Dong Wang, Yu Qiao, and Hongsheng Li. Point-m2ae: multi-scale masked autoencoders for hierarchical point cloud pre-training. In *Advances in neural information processing systems*, 2022.

[43] Zaiwei Zhang, Rohit Girdhar, Armand Joulin, and Ishan Misra. Self-supervised pretraining of 3d features on any point-cloud. *arXiv preprint arXiv:2101.02691*, 2021.